RESEARCH ARTICLE

Key Points:
- Errors in shear wave-splitting azimuths are correlated within any one plate
- Absolute plate velocities differ insignificantly from zero for eight plates
- Seismic anisotropy indicates plate motion direction if speed exceeds ~5 mm a^{-1}

Supporting Information:
- Readme
- Table S1

Correspondence to:
L. Zheng,
linzheng@rice.edu

Absolute plate velocities from seismic anisotropy: Importance of correlated errors

Lin Zheng[1], Richard G. Gordon[1], and Corné Kreemer[2]

[1]Department of Earth Science, Rice University, Houston, Texas, USA, [2]Nevada Bureau of Mines and Geology and Seismological Laboratory, University of Nevada, Reno, Reno, Nevada, USA

Abstract The errors in plate motion azimuths inferred from shear wave splitting beneath any one tectonic plate are shown to be correlated with the errors of other azimuths from the same plate. To account for these correlations, we adopt a two-tier analysis: First, find the pole of rotation and confidence limits for each plate individually. Second, solve for the best fit to these poles while constraining relative plate angular velocities to consistency with the MORVEL relative plate angular velocities. Our preferred set of angular velocities, SKS-MORVEL, is determined from the poles from eight plates weighted proportionally to the root-mean-square velocity of each plate. SKS-MORVEL indicates that eight plates (Amur, Antarctica, Caribbean, Eurasia, Lwandle, Somalia, Sundaland, and Yangtze) have angular velocities that differ insignificantly from zero. The net rotation of the lithosphere is $0.25 \pm 0.11°$ Ma^{-1} (95% confidence limits) right handed about 57.1°S, 68.6°E. The within-plate dispersion of seismic anisotropy for oceanic lithosphere ($\sigma = 19.2°$) differs insignificantly from that for continental lithosphere ($\sigma = 21.6°$). The between-plate dispersion, however, is significantly smaller for oceanic lithosphere ($\sigma = 7.4°$) than for continental lithosphere ($\sigma = 14.7°$). Two of the slowest-moving plates, Antarctica ($v_{RMS} = 4$ mm a^{-1}, $\sigma = 29°$) and Eurasia ($v_{RMS} = 3$ mm a^{-1}, $\sigma = 33°$), have two of the largest within-plate dispersions, which may indicate that a plate must move faster than ≈ 5 mm a^{-1} to result in seismic anisotropy useful for estimating plate motion. The tendency of observed azimuths on the Arabia plate to be counterclockwise of plate motion may provide information about the direction and amplitude of superposed asthenospheric flow or about anisotropy in the lithospheric mantle.

1. Introduction

A long-standing problem in global tectonics is whether "absolute" plate motions, the motions of the plates relative to an external reference frame, usually taken to be the lower mantle, can be usefully estimated. The most widely used method for estimating absolute plate motions has been from the trends (and in some cases the rates of propagation) of hot spot tracks [e.g., *Morgan*, 1972; *Minster et al.*, 1974; *Gripp and Gordon*, 2002; *Morgan and Phipps Morgan*, 2007]. An alternative method for estimating absolute plate motion arises from the orientation of seismic anisotropy inferred from shear wave splitting (mainly from SKS arrivals) [*Becker*, 2008]. The orientations of seismic anisotropy arise from the preferred alignments of highly anisotropic minerals in the asthenosphere, which in many places may indicate the direction of the motion of the lithosphere relative to the subasthenospheric mantle [*Savage*, 1999].

To estimate absolute plate motion, *Kreemer* [2009] compiled 474 orientations from shear wave splitting data. His analysis assumed that errors in the azimuths inferred from shear wave splitting are uncorrelated, which results in confidence limits of ~0.001° Ma^{-1}. Here we test this assumption and find instead that the residuals to azimuths from any one plate are strongly correlated with the residuals from the same plate.

To account for these correlated errors, we develop a new method for analyzing the azimuths inferred from shear wave splitting data. To do so, we adopt a two-tier analysis, similar to the typical method used for analyzing paleomagnetic data [*Irving*, 1964]. First, we find the pole of rotation and confidence limits for each plate individually. Typically, this results in a confidence region that is narrow in one well-constrained direction and elongate in the other. Second, we perform a global inversion in which each plate is represented not by multiple individual estimates of the orientation of seismic anisotropy but by a single best fitting pole and confidence limits. The relative plate angular velocities are constrained to consistency with the MORVEL global set of relative plate angular velocities [*DeMets et al.*, 2010].
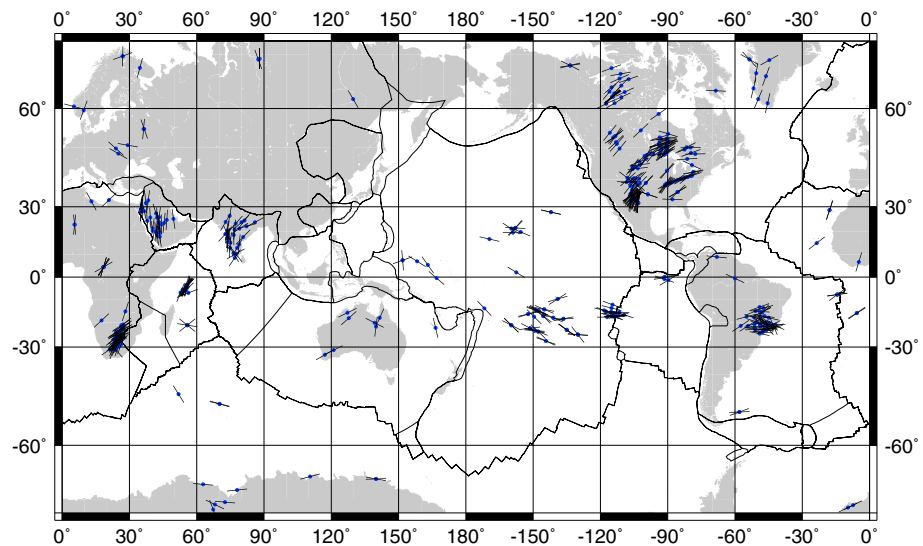
Figure 1. Locations and orientations of shear wave splitting analyzed in this paper.

We apply these new methods to 474 data analyzed by *Kreemer* [2009] except that we omit three problematic data (two from the Pacific plate and one from the Nazca). Thus, we analyze in total 471 orientations inferred from shear wave splitting (Figure 1). Plates are included in the inversion only if the azimuths from anisotropy for that plate differ significantly from what is expected from data drawn from a uniform random distribution in azimuth. This results in the omission of orientations from shear wave splitting from several plates with sparse data. The angular velocities that we determine for those plates are thus inferred from the more populous orientations from other plates and are maximally consistent with globally observed shear wave splitting orientations.

We consider two different approaches to weighting the plates and three different sets of plates to invert: (1) all plates meeting our minimum criteria for the anisotropy data, (2) the oceanic plate subset of the first set, and (3) the continental subset of the first.

The different weighting approaches give results with overlapping confidence limits as do the results from different subsets of data. Our preferred set of angular velocities, SKS-MORVEL, is determined from a subset of the SKS data set from eight plates weighted proportionally to the root-mean-square velocity of each plate and constrained to consistency with the MORVEL global set of relative plate angular velocities. The new set of angular velocities indicates a $0.25 \pm 0.11°$ Ma^{-1} (95% confidence limits here and throughout this paper) right-handed net rotation of the entire lithosphere about 57.1°S, 68.6°E. We conclude that realistic uncertainties in absolute plate motion from seismic anisotropy are $\pm 0.1°$ Ma^{-1} to $\pm 0.2°$ Ma^{-1}, 2 orders of magnitude larger than found before and similar to the formal uncertainties in plate motion relative to the hot spots.

2. Are the Azimuth Errors Uncorrelated?

To test the assumption of uncorrelated errors in the azimuths, we construct a global set of absolute angular velocities in a manner similar to that of *Kreemer* [2009]. We constrain the relative angular velocities to consistency with a predetermined global set of relative plate angular velocities. *Kreemer* [2009] used the mainly geodetically constrained plate motion model of *Kreemer et al.* [2006], while here we use the more recently determined MORVEL global set of relative plate angular velocities [*DeMets et al.*, 2010]. With this constraint, we determined a least squares fit to all azimuths while treating them not as strikes, but as trends (i.e., as polar vectors rather than axial vectors). This requires choosing which of the two antipodal directions to use as the unique direction of plate motion for each datum. We exactly followed the choices made by *Kreemer* [2009] (except that we corrected a few transcription

errors in azimuths and a few errors in plate assignment) and applied the trend-fitting function of *Chase* [1972] as implemented by *DeMets et al.* [1990].

We find a new global set of plate angular velocities relative to the subasthenospheric mantle, SKS-UNCOR-MORVEL, from a grid search for *r*, the minimum sum-squared normalized error:

$$r = \sum_{i=1}^{N} \left(\frac{2}{\sigma_i} \sin \frac{\alpha_i}{2} \right)^2 \tag{1}$$

where σ_i is the uncertainty of an azimuth inferred from shear wave splitting. We assign the same uncertainty for each shear wave splitting azimuth in the SKS data set. For the purposes of estimating plate motion, sources of uncertainty in azimuth include measurement error, anisotropy from the mantle lithosphere as is inferred, for example, for North America [*Yuan and Romanowicz*, 2010], and pressure-gradient- or density-driven flow in the asthenosphere [*Conrad et al.*, 2007; *Conrad and Behn*, 2010].

Following the procedure of *Kreemer* [2009], in constructing SKS-UNCOR-MORVEL, we assume that the errors are uncorrelated. α_i is the angular difference between the orientation of the observed shear wave splitting and the azimuth calculated from the plate angular velocities. Due to the 180° ambiguity of the azimuth of shear wave splitting, α_i varies from −90° to 90°.

The resulting set of angular velocities, which we refer to as SKS-UNCOR-MORVEL, are similar to those obtained by *Kreemer* [2009], and the 95% confidence limits on the angular velocity are about a factor of 3 larger (±0.006° Ma^{-1} 3-D 95% confidence limits), mainly because we assigned larger errors to the data to be consistent with their dispersion. The confidence limits that we determine with this approach are nevertheless nearly 2 orders of magnitude smaller than the confidence limits estimated from hot spot tracks [e.g., *Gripp and Gordon*, 2002].

To examine whether the errors are uncorrelated, we analyze the azimuth residuals for each plate separately (Figures 2a–2k). If the azimuth errors were uncorrelated within each plate, the mean direction of the azimuth residuals of any single plate would be expected to differ insignificantly from zero. Because an azimuth residual of θ and an azimuth residual of $\theta + 180°$ are indistinguishable, we eliminate this ambiguity by doubling the azimuth residuals so that the axial data are transformed to circular data [*Mardia and Jupp*, 1999]. Let $\varphi(\theta) = 2\theta$. It follows that $\varphi(\theta + 180°) = 2\theta + 360°$, which is equivalent to 2θ. Thus, θ and $\theta + 180°$ are treated equivalently. The mean direction of these doubled azimuth residuals is then determined [*Mardia and Jupp*, 1999].

Given the azimuth residuals $\theta_1, \theta_2, \dots \theta_N$, the mean direction, $\overline{\varphi}$, of the doubled azimuth residuals is

$$\overline{\varphi} = \begin{cases} \tan^{-1}\left(\overline{C}/\overline{S}\right) & \text{if } \overline{C} \geq 0 \\ \tan^{-1}\left(\overline{C}/\overline{S}\right) + 180° & \text{if } \overline{C} < 0 \end{cases} \tag{2}$$

where $\overline{C} = \frac{1}{N} \sum_{i=1}^{N} \cos\varphi_i$, $\overline{S} = \frac{1}{N} \sum_{i=1}^{N} \sin\varphi_i$, and $\varphi_i = 2\theta_i$ [*Mardia and Jupp*, 1999]. $\sigma\overline{\varphi}$, the standard error (i.e., standard deviation of the mean), is estimated by the sample circular standard deviation σ_φ divided by the square root of the sample size *N*:

$$\sigma\overline{\varphi} = \frac{\sigma_\varphi}{\sqrt{N}} = \frac{\sqrt{-2\ln\overline{R}}}{\sqrt{N}} \tag{3}$$

where the mean resultant length $\overline{R} = \sqrt{\overline{C}^2 + \overline{S}^2}$.

To obtain $\overline{\theta}$, the mean direction of the azimuth residuals, and $\sigma\overline{\theta}$, the standard error of the mean, $\overline{\varphi}$ and $\sigma\overline{\varphi}$ are respectively halved. Among the 11 plates with azimuth data in SKS-UNCOR-MORVEL, the mean directions of azimuth residuals for five plates (the Arabia, Australia, North America, Nubia, and Pacific plates) differ significantly (at the 95% confidence level) different from zero (Table 1). The difference from zero of the mean residuals ranges in magnitude from 2.0° ± 7.2° for the South America plate to 25.6° ± 3.8° for the Arabia plate. If the errors were uncorrelated, the probability of five or more plates out of 11 plates differing significantly from zero is only 1.1×10^{-4} [*Wadsworth*, 1960]. Therefore, the hypothesis of uncorrelated errors in the azimuths can be rejected.
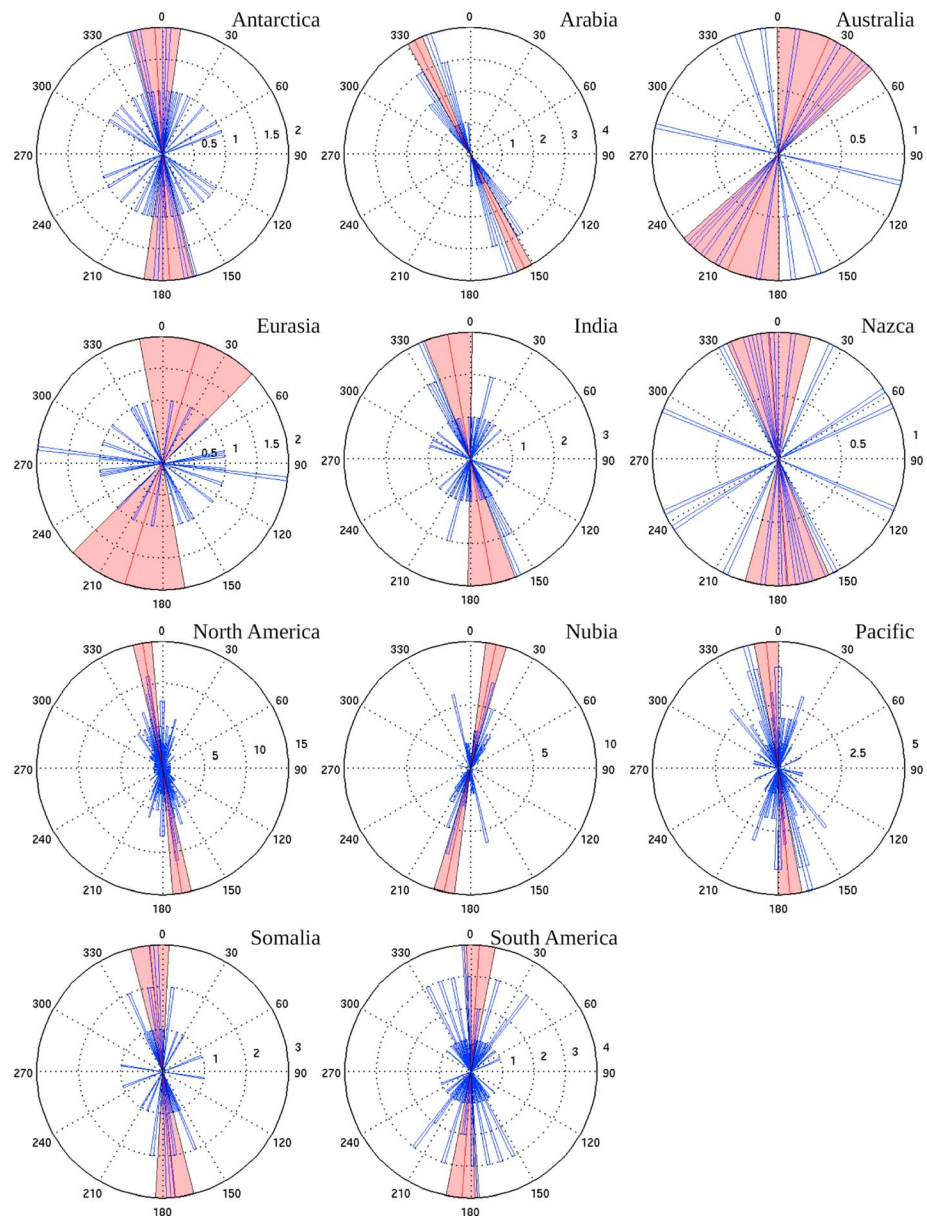
Figure 2. Rose diagrams of azimuth residuals (the difference between the observed orientations of shear wave splitting and the orientations calculated from SKS-UNCOR-MORVEL). The blue bars indicate the distribution of azimuth residuals. The red thick lines show the mean direction of azimuth residuals. The red-shaded region shows the 95% confidence limit of the mean direction. The mean directions of azimuth residuals for each plates are Antarctica plate, $-6.8° \pm 13.0°$ (95% confidence limit, hereinafter c.l.), insignificantly different from zero ($p = 30.4\%$); Arabia plate, $-25.6° \pm 3.7°$ (95% c.l.), significantly different from zero ($p = 7.9 \times 10^{-41}$); Australia plate, $24.0° \pm 23.8°$ (95% c.l.), significantly different from zero ($p = 4.8\%$); Eurasia plate, $12.0° \pm 27.7°$ (95% c.l.), insignificantly different from zero ($p = 39.7\%$); India plate, $-9.8° \pm 10.8°$ (95% c.l.), insignificantly different from zero ($p = 7.4\%$); Nazca plate, $-2.5° \pm 19.2°$ (95% c.l.), insignificantly different from zero ($p = 79.8\%$); North America plate, $-12.9° \pm 4.2°$ (95% c.l.), significantly different from zero ($p = 1.1 \times 10^{-9}$); Nubia plate, $14.3° \pm 4.7°$ (95% c.l.), significantly different from zero ($p = 3.0 \times 10^{-9}$); Pacific plate, $-5.8° \pm 5.5°$ (95% c.l.), significantly different from zero ($p = 3.7\%$); Somalia plate, $-6.0° \pm 8.7°$ (95% c.l.), insignificantly different from zero ($p = 17.7\%$); South America plate, $2.0° \pm 7.1°$ (95% c.l.), insignificantly different from zero ($p = 58.4\%$).

Table 1. Statistics of the Azimuth Residuals for SKS-UNCOR-MORVEL[a]

Plate Name	N	$\bar{\theta}$	σ_θ	$\sigma_{\bar{\theta}}$	p
Antarctica	24	−6.8°	32.6°	6.6°	30.4%
Arabia	25	−25.6°	9.6°	1.9°	**7.9 × 10^{-41}**
Australia	8	24.0°	34.3°	12.1°	**4.8**%
Eurasia	13	12.0°	50.9°	14.1°	39.7%
India	28	−9.8°	29.1°	5.5°	7.4%
Nazca	9	−2.5°	33.9°	9.8°	79.8%
North America	164	−12.9°	27.1°	2.1°	**1.1 × 10^{-9}**
Nubia	59	14.3°	18.5°	2.4°	**3.0 × 10^{-9}**
Pacific	65	−5.8°	22.5°	2.8°	**3.7**%
Somalia	24	−6.0°	21.8°	4.4°	17.7%
South America	52	2.0°	26.0°	3.6°	58.4%

[a]N is the number of orientations of shear wave splitting on each plate. $\bar{\theta}$ is the mean direction of the azimuth residuals, σ_θ is the standard deviation, and $\sigma\bar{\theta}$ is the standard error. $\bar{\theta}$, σ_θ, and $\sigma_{\bar{\theta}}$ are found by halving $\bar{\varphi}$, σ_φ, and σ_φ, respectively. p is the significance level at which the mean direction of azimuth residuals differs from zero. Probabilities less than 5% are printed in bold, which indicate that the differences are statistically significant. In total, there are 471 observed orientations of shear wave spitting and the global sample circular standard deviation, σ_θ, is 28.4°.

3. Two-Tier Analysis

We follow procedures analogous to standard practice in the analysis of paleomagnetic data [e.g., *Irving*, 1964]; i.e., our analysis has two tiers. First, we estimate a pole of rotation for each plate individually that best fits the azimuths from that plate. Second, we solve for a globally self-consistent set of angular velocities constrained to consistency with the MORVEL global set of relative plate angular velocities [*DeMets et al.*, 2010].

3.1. Best Fitting Pole for Each Plate

To estimate the best fitting pole for each individual plate, we follow the same procedure as described above to estimate SKS-UNCOR-MORVEL while using only the shear wave splitting orientations from that one plate (Table 2a and Figure 4). Because the underlying data are not trends (i.e., a polar vector), but strikes (an axial vector), a pole and its antipode fit the observed shear wave splitting orientations equally well. For example, on the Arabia plate there are 25 shear wave splitting orientations incorporated in our SKS data set. The individual best fitting pole for the Arabia plate estimated from these 25 orientations is located at 10.9°S, 68.0°W or 10.9°N, 112.0°E.

Table 2a. Statistics of Azimuth Residuals With Respect to the Individual Best Fitting Pole[a]

Plate Name	N	N_{OC}	Individual Best Fitting Pole		σ	ax1	ax2	azi	S	p
Antarctica	24	3	−81.9°N	19.2°E	28.7°	3.0°	1.4°	116°	14.8	**6.2 × 10^{-4}**
Arabia	25	0	−10.9°N	292.0°E	7.3°	18.0°	1.3°	68°	57.2	**3.8 × 10^{-13}**
Australia	8	1	−1.2°N	285.9°E	29.7°	23.7°	6.3°	45°	6.1	4.8%
Eurasia	13	0	−59.4°N	236.6°E	32.6°	4.6°	3.1°	94°	5.4	6.8%
India	28	0	−12.4°N	272.5°E	22.2°	3.6°	1.3°	69°	32.4	**9.2 × 10^{-8}**
Nazca	9	9	−67.1°N	71.7°E	15.7°	26.7°	5.1°	7°	16.0	**3.4 × 10^{-4}**
North America	164	0	−13.2°N	103.1°E	22.3°	3.7°	1.1°	26°	180.6	**<1 × 10^{-16}**
Nubia	59	5	−30.7°N	147.2°E	17.9°	4.7°	1.7°	65°	90.1	**<1 × 10^{-16}**
Pacific	65	65	−66.6°N	87.1°E	21.1°	6.8°	2.7°	129°	80.0	**<1 × 10^{-16}**
Somalia	24	24	−0.2°N	227.4°E	17.7°	4.3°	0.6°	57°	37.6	**6.7 × 10^{-9}**
South America	52	5	−81.4°N	143.4°E	23.7°	20.9°	3.2°	170°	52.0	**5.1 × 10^{-12}**
Global	471	112			21.3°					
Selected plates	426	108			20.4°					

[a]N is the number of orientations of shear wave splitting on that plate. N_{OC} is the number of orientations of shear wave splittings beneath oceanic crust. σ is standard deviation. ax1 is the 1σ one-dimensional length of the long axis, ax2 is the length of the short axis, and azi is the azimuth of the long axis of the confidence ellipse for the individual best fitting pole. S is the modified Rayleigh statistic, which indicates the likelihood of the azimuth is drawn from a uniform random distribution. p is the significance level at which the azimuth residuals differs from a uniform random distribution. Probabilities less than 5% are printed in bold, which indicate that the differences are statistically significant. The line labeled "Global" is the full data set used in *Kreemer* [2009]; the line labeled "Selected plates" is the selected data set after removing the data from the Antarctica, Australia, and Eurasia plates.
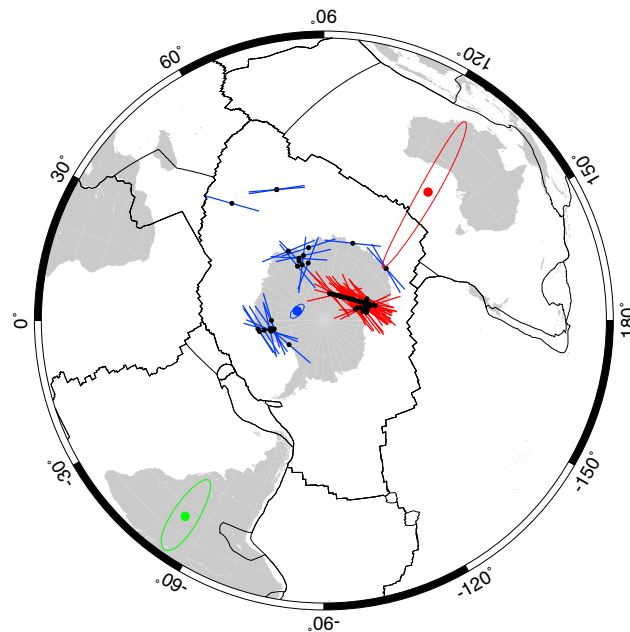
Figure 3. Observed orientations of shear wave splitting for the Antarctica plate. Blue lines, SKS data used by *Kreemer* [2009]; red lines, SKS data from the Transantarctic Mountain [*Barklage et al.*, 2009]; blue dot and ellipse, individual best fitting pole (81.9°S, 19.2°E) of the Antarctica plate and 95% confidence limit (long axis 2.3° with the azimuth of 116° and short axis of 1.2°) constrained by the SKS data used by *Kreemer* [2009]; red dot and ellipse, individual best fitting pole (41.2°S, 129.1°E) and 95% confidence limit (long axis 26.5° with the azimuth of 172° and short axis of 2.3°) constrained by the SKS data determined by *Barklage et al.* [2009]; green dot and ellipse, individual best fitting pole (16.2°S, 305.3°E) and 95% confidence limit (long axis 14.8° with the azimuth of 178° and short axis of 3.0°) constrained by a combined SKS data set from both *Kreemer* [2009] and *Barklage et al.* [2009]. Lambert azimuthal equal-area projection.

3.2. Are the Azimuths Drawn From a Uniform Random Distribution?

The modified Rayleigh statistic can be used to test if the azimuth residuals from any one plate differ significantly from a uniform distribution [*Mardia and Jupp*, 1999]. As above, the angles of azimuth residuals are doubled. The modified Rayleigh statistic S is given by

$$S = \left(1 - \frac{1}{2N}\right) 2N\bar{R}^2 + \frac{N\bar{R}^4}{2} \qquad (4)$$

where the mean resultant length is given by

$$\bar{R} = \frac{1}{N}\left(\left(\sum_{i=1}^{N}\cos\theta_i\right)^2 + \left(\sum_{i=1}^{N}\sin\theta_i\right)^2\right)^{\frac{1}{2}} \qquad (5)$$

The modified Rayleigh statistic S has an approximately χ^2 distribution [*Mardia and Jupp*, 1999; *Jupp*, 2001].

For seven of the 11 plates, the Rayleigh test shows that the probabilities of the azimuth residuals being drawn from a uniform random distribution are remote ($p \leq 9 \times 10^{-8}$) and we accept these seven plates for further analysis (Table 2a). The remaining four plates, Antarctica ($N = 24$, $p = 6.2 \times 10^{-4}$), Australia ($N = 8$, $p = 0.048$), Eurasia ($N = 13$, $p = 0.068$), and Nazca ($N = 12$, $p = 3.4 \times 10^{-4}$), require further discussion. The combination of few data and marginal probability of being drawn from a uniform random distribution lead us to reject the results for Australia and Eurasia. The low probability of the Nazca plate data being drawn from a random distribution leads us to tentatively accept the Nazca plate for further analysis. From just the statistics, we would also tentatively accept the Antarctica plate, but a more detailed analysis below causes us to reject the data from Antarctica.

3.3. Azimuths From Antarctica

Aside from a couple of oceanic data, the Antarctica data used by *Kreemer* [2009] are from sites along or near the Antarctic coastline and tend to strike parallel to the coast, raising questions as to whether they parallel plate motion or reflect anisotropy in the lithosphere (Figure 3). Azimuths from shear wave splitting observed along the Transantarctic Mountains by *Barklage et al.* [2009] (and unavailable to *Kreemer* [2009]) tend to parallel the strike of the mountains (Figure 3). The pole of rotation and 95% confidence limits fit to the Transantarctic Mountain data differs significantly from the pole (and confidence region) determined for *Kreemer's* [2009] Antarctica data (Figure 3). Thus, the seismic anisotropy recorded along the Transantarctic Mountains is not consistent with recording the same plate motion as indicated by the data from near the coast. We conclude that it is difficult to interpret the shear wave splitting data used by *Kreemer* [2009] from Antarctica in terms of the direction of motion of the Antarctica plate and thus we omit these data from our global inversion.

3.4. Another Test of the Hypothesis of Uncorrelated Errors

We incorporate the shear wave splitting data from eight plates (Arabia, India, Nazca, North America, Nubia, Pacific, Somalia, and South America) in our analysis of global absolute plate motions. For each plate, there are two antipodal best fitting rotation poles relative to the subasthenospheric mantle (Figure 4 and Table 2a).
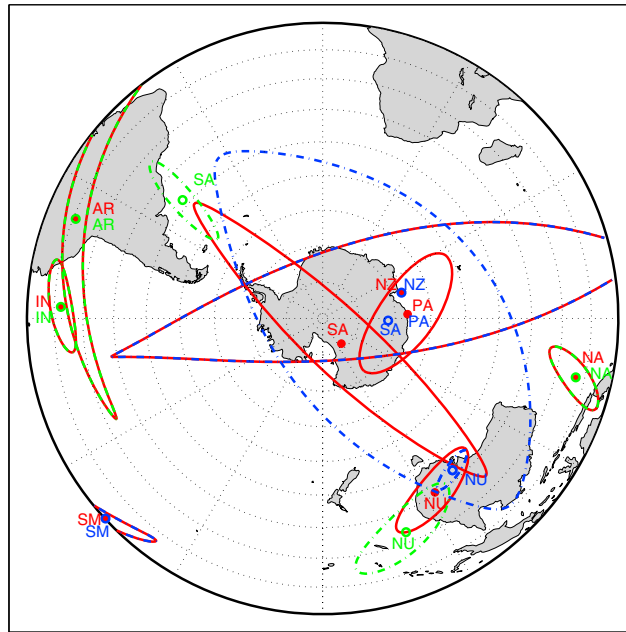
Figure 4. The location and 95% confidence limits of the individual best fitting poles. Blue denotes individual poles estimated from the oceanic data set; green denotes individual poles estimated from the continental data set; red denotes individual poles estimated from the combined data set. Lambert azimuthal equal-area projection.
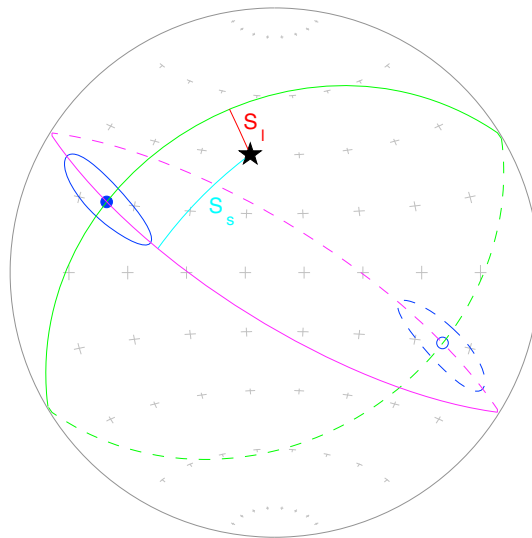

Figure 5. Estimate a global set of best fitting angular velocities from the rotation poles which fit each individual plate. The blue solid and open dots show a pair of antipoles, which fit the orientations of observed shear wave splitting on one plate. The black star shows the corresponding best fitting angular velocity in our global set. The magenta solid and dash lines show the great circle perpendicular to the short axes of the uncertainty ellipses of this pair of antipoles. The green solid and dash lines show the great circle perpendicular to the long axes. The red solid line shows the s_{l_i} distance starting from the best fitting pole in global set to the great circle perpendicular to the long axes. The cyan solid line shows s_{s_i}, the distance starting from the best fitting pole in global set to the great circle perpendicular to the short axes.

A global set of angular velocities relative to the subasthenospheric mantle was determined from a grid search for the minimum weighted least squares error, r, while constraining the relative plate angular velocities to consistency with MORVEL [*DeMets et al.*, 2010]:

$$r = \sum_{i=1}^{2n} \left(\frac{s_i}{\sigma_i}\right)^2 \qquad (6)$$

where σ_i is the length of the short (or long) semiaxis of the uncertainty ellipse of an individual best fitting pole, s_i is the distance starting from the corresponding trial pole of rotation in our global set to a great circle which is perpendicular to the corresponding axis, and n is the number of plates (Figure 5). This equation is identical to the fitting function to paleomagnetic poles with elliptical confidence limits adopted by *Gordon and Cox* [1980]. The size of the uncertainty ellipse for an individual best fitting pole is the same as that for its antipode, and the great circle perpendicular to the long axis of an individual pole is also perpendicular to the long axis of its antipode (Figure 5). (In other words, s_i is the same for an antipodal pair.). Thus, the sum-squared normalized misfit determined from equation (6) is identical for either antipode, and therefore, this least squares analysis requires no preselection between a pole and its antipode.

If the errors were uncorrelated, we could simply use the lengths of the semiaxes found above in equation (6). When we do so, we find a value for r of 990 with 13 degrees of freedom. The probability of obtaining a value of r this large or larger is less than 1×10^{-16}, and the hypothesis of uncorrelated errors can be rejected.

3.5. Global Set of Angular Velocities From Equal Weighting

The sizes of the uncertainty ellipses can be normalized such that the short axes of different plates are given equal weight. We refer to the resulting global set of angular velocities as SKS-GE-MORVEL (Figures 6 and 7).
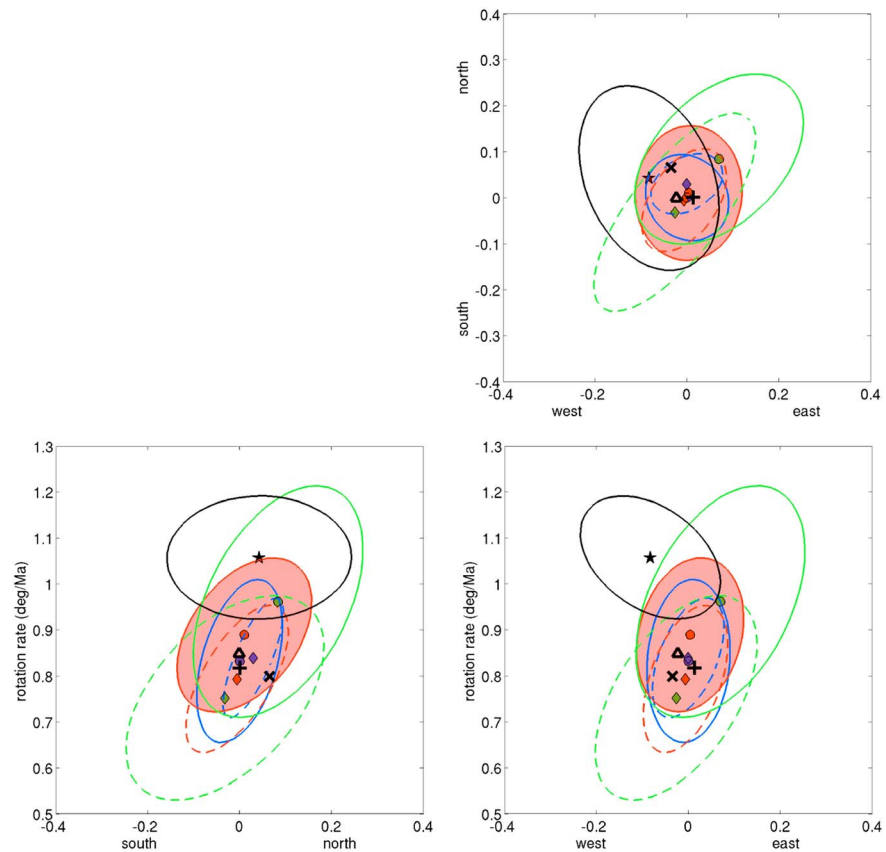
Figure 6. Angular velocity of the Pacific plate relative to the subasthenospheric mantle. Ellipses are 3-D 95% confidence limits. Red-filled diamond with red dashed confidence limits, SKS-GE-MORVEL (all plates, equal weighted); red-filled circle with solid red confidence limit (also shaded in red), SKS-MORVEL (equivalent to SKS-GV-MORVEL; all plates, v_{RMS} weighted); blue-filled diamond with blue dashed confidence limits, SKS-OE-MORVEL (oceanic plates, equal weighted); blue-filled circle with solid blue confidence limits, SKS-OV-MORVEL (oceanic plates, v_{RMS} weighted); green diamond with dashed green confidence limits, SKS-CE-MORVEL (continental plates, equal weighted); green-filled circle with solid green confidence limits, SKS-CV-MORVEL (continental plates, v_{RMS} weighted); black star with solid black confidence limits, HS3-NUVEL1A [*Gripp and Gordon*, 2002]; black plus sign, SKS-UNCOR-MORVEL; black cross, Pacific plate angular velocity of *Morgan and Phipps Morgan* [2007]; black triangle, Pacific angular velocity of *Kreemer* [2009].

3.6. Alternative Weighting

The assumption that asthenospheric lattice-preferred orientation is always parallel to absolute plate motions may be more valid beneath fast-moving plates than beneath slow-moving plates, because the density-driven asthenospheric flow has a proportionally larger effect on the observed seismic anisotropy when the plate velocities are low [*Conrad et al.*, 2007; *Conrad and Behn*, 2010]. If all errors in observed orientations of shear wave splitting were due to the superposed asthenospheric flow, the faster-moving plates should be given more weight in a global inversion than the slower-moving plates.

The root-mean-square velocities, v_{RMS}, of the eight plates (Arabia, India, Nazca, North America, Nubia, Pacific, Somalia, and South America) with useful anisotropy data range from 17 to 79 mm a^{-1} in SKS-GE-MORVEL (Table S1 in the supporting information). We use these as initial input for determining a set of angular velocities for which the short axis of the confidence ellipse of each input pole of rotation is weighted by v_{RMS}. We estimate a global set of angular velocities via a grid search for the minimum weighted least squares error as in equation (6) except that we replace σ_i with ζ_i:

$$\zeta_i = \sigma_i c / v_i \qquad (7)$$

where v_i is v_{RMS} of the plate of interest, σ_i is equal for all short semiaxes with the value for the long semiaxes chosen to preserve the aspect ratio of each ellipse, and c is a plate-independent constant that is adjusted ex post facto such that r equals the numbers of degrees of freedom.
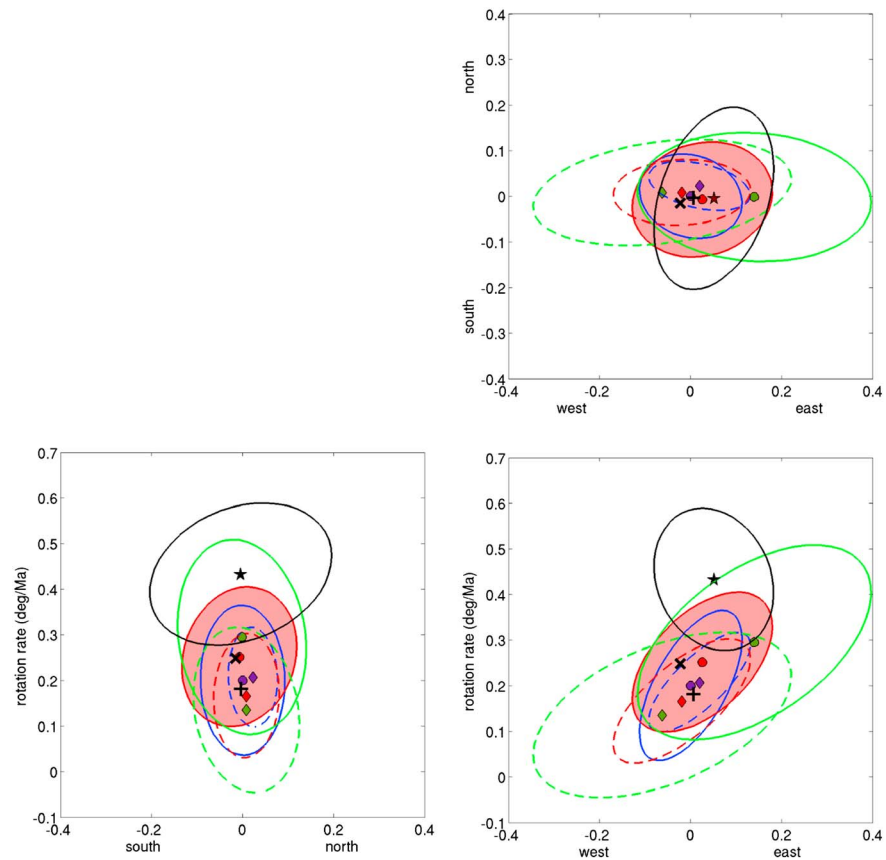
Figure 7. The net rotation of the lithosphere relative to the subasthenospheric mantle. Ellipses are 3-D 95% confidence limits. Red diamond with dashed confidence limits, SKS-GE-MORVEL (all plates, equal weighted); red circle with red solid confidence limits (also shaded in red), SKS-MORVEL (equivalent to SKS-GV-MORVEL; all plates, v_{RMS} weighted); blue diamond with dashed blue confidence limits, SKS-OE-MORVEL (oceanic plates, equal weighted); blue circle with solid blue confidence limits, SKS-OV-MORVEL (oceanic plates, v_{RMS} weighted); green diamond with dashed green confidence limits, SKS-CE-MORVEL (continental plates, equal weighted); green circle with solid green confidence limits, SKS-CV-MORVEL (continental plates, v_{RMS} weighted); black star with black solid confidence limits, HS3-NUVEL1A [*Gripp and Gordon*, 2002]; black plus sign, SKS-UNCOR-MORVEL; black cross, net rotation estimated by *Cocksworth and Harper* [1996]. Ellipses show the 3-D 95% confidence limits.

In the resulting set of angular velocities, SKS-GV-MORVEL, which differ insignificantly from SKS-GE-MORVEL, the angular velocity of the Pacific plate is $0.89 \pm 0.12°$ Ma^{-1} right handed about 63.4°S, 100.3°E (Table 4 and Figures 6 and 7), which is 0.10° Ma^{-1} larger than the angular velocity indicated by SKS-GE-MORVEL (64.5°S, 98.7°E, $0.79 \pm 0.11°$ Ma^{-1}). SKS-GV-MORVEL is our preferred set of absolute angular velocities, and hereinafter, we refer to this set simply as SKS-MORVEL.

3.7. Continental Subset and Oceanic Subset

Among the eight plates used in SKS-GE-MORVEL, three plates (the Pacific, Nazca, and Somalia plates) have estimates of seismic anisotropy from only oceanic lithosphere, three plates (the Arabia, India, and North America plates) have only continental data, and two plates (the Nubia and South America plates) have both.

Anisotropy in the lithosphere may cause the observed orientations of shear wave splitting beneath continental crust to deviate significantly from the directions of asthenospheric flow [*Silver*, 1996; *Savage*, 1999; *Silver et al.*, 2001, 2004, 2006; *Fouch and Rondenay*, 2006; *Marone and Romanowicz*, 2007; *Conrad et al.*, 2007; *Yuan and Romanowicz*, 2010; *Long and Becker*, 2010]. In contrast, the highest rates of mantle flow due to return flow from trenches to ridges [*Chase*, 1979] or due to buoyancy-driven flow [*Behn et al.*, 2004; *Conrad and Behn*, 2010] may occur under oceanic plates. Thus, we determine, compare, and contrast plate motions inferred from oceanic-only shear wave splitting data with plate motions inferred from continental-only shear wave splitting and compare both with plate motions inferred above from global data.

Table 2b. Statistics of Azimuth Residuals Respect to the Individual Best Fitting Pole for Oceanic and Continental Subsets[a]

Plate Name	N	Individual Best Fitting Pole		σ	ax1	ax2	azi	S	p
Nubia	5	−32.9°N	139.5°E	2.2°	1.3°	0.5°	71°	11.4	**0.3**%
South America	5	−72.0°N	91.7°E	15.4°	14.9°	6.9°	47°	10.1	**0.6**%
Oceanic subset	111			19.2°					
Nubia	54	−23.5°N	158.7°E	18.2°	5.3°	2.1°	57°	80.9	**$<1\times10^{-16}$**
South America	47	−37.9°N	310.2°E	23.0°	5.7°	1.1°	7°	49.7	**1.6×10^{-11}**
Continental subset	318			21.6°					

[a]N is the number of orientations of shear wave splitting on that plate. N_{OC} is the number of orientations of shear wave splittings beneath oceanic crust. σ is standard deviation. ax1 is the 1σ one-dimensional length of the long axis, ax2 is the length of the short axis, and azi is the azimuth of the long axis of the confidence ellipse for the individual best fitting pole. S is the modified Rayleigh statistic, which indicates the likelihood of the azimuth is drawn from a uniform random distribution. p is the significance level at which the azimuth residuals differs from a uniform random distribution. Probabilities less than 5% are printed in bold, which indicate that the differences are statistically significant. Oceanic subset and continental subset are the seismic anisotropy observed beneath oceanic and continental lithosphere, respectively.

Figure 4 shows the individual best fitting poles estimated from the continental subset and from the oceanic subset. For the Nubia and South America plates, the oceanic pole and continental pole are similar to one another but nonetheless differ significantly from one another, and the best fitting pole estimated from the combined data lies between the oceanic and continental poles.

We follow the same procedures described above. We refer to the resulting four global sets of absolute angular velocities as SKS-OE-MORVEL (oceanic data with each plate equally weighted), SKS-OV-MORVEL (oceanic data with each plate weighted by its root-mean-square velocity), SKS-CE-MORVEL (continental data with each plate equally weighted), and SKS-CV-MORVEL (continental data with each plate weighted by its root-mean-square velocity) (Figures 6 and 7 and Tables 2b and S1).

The angular speed of the Pacific plate ranges from $0.75 \pm 0.15°$ Ma^{-1} in SKS-CE-MORVEL to $0.97 \pm 0.19°$ Ma^{-1} in SKS-CV-MORVEL (Tables 4 and S1). The angular velocities estimated from the two different weighting approaches differ insignificantly when using the same data set. The angular velocities constrained by alternative data sets differ insignificantly from each other (Figures 6 and 7). Compared with the angular velocity constrained by continental data, the angular velocity constrained by oceanic data is less sensitive to the choice of weighting approach. Moreover, the confidence limits of the angular velocities constrained by oceanic data are always more compact than those constrained by continental data (Figures 6 and 7).

Table 3 shows that the between-plate dispersion is significantly higher for the continents (short axis $\sigma_b = 14.7°$) than for the oceans (short axis $\sigma_b = 7.4°$; $F = 3.93$ with 7 versus 7 degrees of freedom; $p = 4.6\%$). This difference may be caused by greater anisotropy in continental lithosphere relative to oceanic lithosphere. Alternatively, but probably less likely (as we include oceanic lithosphere from Somalia and South America), the greater dispersion between continents may be because continents tend to move more slowly than oceanic plates and thus their azimuths are more sensitive to asthenospheric flow not caused by shearing from plate motion.

Table 3. Comparisons of Best Fitting Angular Velocities Estimated From Various Data Sets and Weighting Approaches[a]

Data Set	Pacific			Net Rotation			
	°N	°E	°Ma^{-1}	°N	°E	°Ma^{-1}	σ
SKS-UNCOR-MORVEL	−64.0	101.9	0.8178	−57.0	61.6	0.1818	
SKS-GE-MORVEL	−64.5	98.7	0.7929	−52.6	46.8	0.1673	11.5°
SKS-GV-MORVEL	−63.4	100.3	0.8890	−57.1	68.6	0.2529	
SKS-OE-MORVEL	−62.1	99.6	0.8395	−49.4	66.1	0.2092	7.4°
SKS-OV-MORVEL	−64.1	99.8	0.8320	−55.9	58.0	0.1999	
SKS-CE-MORVEL	−66.5	94.6	0.7529	−46.0	20.6	0.1491	14.7°
SKS-CV-MORVEL	−59.8	107.8	0.9673	−48.7	98.4	0.3263	

[a]Pacific is the angular velocity of the Pacific plate relative to the subasthenospheric mantle. Net rotation describes the net angular velocity of the entire lithosphere relative to the subasthenospheric mantle. For equally weighted approach, σ is defined as the length of the short axes. Shear wave splitting data set abbreviations are as follow: UNCOR, single-tier analysis in which each azimuth from shear wave splitting is given unit weight assuming uncorrelated errors; GE, all plates, equally weighted; GV, all plates, RMS velocity weighted; OE, oceanic plates, equally weighted; OV, oceanic plates, RMS velocity weighted; CE, continental plates, equally weighted; CV, continental plates, RMS velocity weighted.

4. Discussion

4.1. Data Dispersion and its Possible Relation to Plate Speed

The observed dispersion of azimuths inferred from seismic anisotropy may provide information on the processes that influence anisotropy. The global average of within-plate standard deviation of the azimuths of seismic anisotropy is 21.3° (Table 2a). Unsurprisingly, this is significantly less than 28.4° (Table 1), the standard deviation found when the global data were inverted assuming uncorrelated errors. Presumably, the latter includes a contribution from the between-plate dispersion and from the unequal weighting of the plates owing to the large number of data from a few plates: Nubia, South America, Pacific, and especially North America.

The variation of within-plate dispersion between plates is significant and large, ranging from $\sigma = 7.3°$ for Arabia to $\sigma = 32.6°$ for Eurasia. The standard deviation of Arabia is significantly lower than that of all (10) other plates. Perhaps, it is low because a relatively small geographic area is sampled, but we note that only a slightly larger area is sampled in the India and Somalia plates for which the within-plate dispersion is comparable to most other plates.

The best-determined standard deviation for an individual plate is that for North America ($\sigma = 15.7°$, $N = 164$). The within-plate dispersion for all continental lithosphere ($\sigma = 21.6°$) differs insignificantly from the within-plate dispersion for all oceanic lithosphere ($\sigma = 19.2°$, $F = 1.27$ with 302 versus 101 degrees of freedom, $p = 0.08$).

The standard deviation of the misfits of the orientations for Eurasia is significantly larger than that of seven other plates although Eurasia's standard deviation is determined from only 13 data. Perhaps the greater dispersion is a consequence of the very slow motion relative to the mantle that we infer for Eurasia; its v_{RMS} of 3 mm a^{-1} differs insignificantly from zero (Table 4 and Figures 9 and 10). The slow motion of Antarctica, with a v_{RMS} of 4 mm a^{-1} that differs insignificantly from zero (Table 4), may also help to explain its relatively high dispersion of orientations as well. In contrast, Nubia ($v_{RMS} = 9$ mm a^{-1}) moves 2 or 3 times as fast as Eurasia or Antarctica and does not have a high dispersion (Table 4). (Nubia moves faster than Eurasia and Antarctica in all our sets of angular velocities except SKS-CV-MORVEL). So perhaps a plate must be moving faster than ~5 mm a^{-1} over millions of years to result in seismic anisotropy that can be used to estimate its direction of plate motion [*Zhang and Karato*, 1995; *Tommasi et al.*, 1999].

This threshold is lower than the threshold that has been suggested by prior workers for the development of seismic anisotropy in the asthenosphere. For example, *Debayle et al.* [2005] conclude that of all Earth's continents, only the continental portion of the Australian plate displays azimuthal anisotropy strongly correlated with current plate motion and that it is due to its relatively high plate speed ($v_{RMS} = 69$ mm a^{-1}, Table 4) relative to the subasthenospheric mantle. We suggest that their estimates of correlation may have been hampered by the use of a no net rotation reference frame rather than a hot spot reference frame.

In contrast, *Marone and Romanowicz* [2007] find that at asthenospheric depths beneath North America ($v_{RMS} = 23$ mm a^{-1}, Table 4), the fast axis of seismic anisotropy is parallel to absolute plate motion as indicated by the plate-hot spot angular velocities of *Gripp and Gordon* [2002], while *Adam and Lebedev* [2012] find that at asthenospheric depths beneath southern Africa ($v_{RMS} \approx 10$ mm a^{-1} for the Lwandle, Nubia, or Somalia plate, Table 4) that the fast axis of seismic anisotropy is parallel to absolute plate motion as indicated by the Africa-hot spot angular velocity of *Gripp and Gordon* [1990].

Recently, *Debayle and Ricard* [2013] find that the amplitude of seismic anisotropy projected onto the direction of current plate motion relative to the hot spots [*Gripp and Gordon*, 1990] is very weak for plate speeds <30 mm a^{-1}, increases significantly between 30 mm a^{-1} and 50 mm a^{-1}, and saturates for plate velocities > 50 mm a^{-1}.

While our analysis does not consider the amplitude of seismic anisotropy, our results indicate that the distribution of azimuths of the fast direction can be interpreted in terms of a pole of absolute motion for each of several continental plates moving slower than 30 mm a^{-1}. We can exclude the resulting residuals as being from a uniform random distribution for many intermediate and slowly moving continental plates including Arabia ($v_{RMS} = 29$ mm a^{-1}), India ($v_{RMS} = 44$ mm a^{-1}), North America ($v_{RMS} = 23$ mm a^{-1}), Nubia ($v_{RMS} = 9$ mm a^{-1}), Somalia ($v_{RMS} = 13$ mm a^{-1}), and South America ($v_{RMS} = 26$ mm a^{-1}) (Tables 2a and 4). While there are other possible explanations for these coherent plate-scale spatial patterns of seismic anisotropy, these results suggest that motion as slow as ≈ 9 mm a^{-1} may be fast enough to organize the simple shearing believed to be responsible for asthenospheric seismic anisotropy.

Table 4. Angular Velocities of SKS-MORVEL[a]

Plate	Angular Velocity			Standard Error Ellipse			σ_ω °/Ma^{-1}	v_{RMS} mm a^{-1}	$p(\chi^2)_0$
	°N	°E	°/Ma^{-1}	σ_{max}	σ_{min}	ζ_{max}			
Major plates									
Amur	62.8	146.2	0.0595	58.3	45.5	32	0.0400	2.5	51.8%
Antarctica	22.6	88.2	0.0392	65.7	54.6	154	0.0530	3.8	88.4%
Arabia	26.4	10.1	0.4691	11.2	6.8	111	0.0469	29.3	$<1\times10^{-16}$
Australia	12.2	44.2	0.6613	8.2	4.8	124	0.0454	68.6	$<1\times10^{-16}$
Caribbean	−22.8	290.4	0.1224	34.3	25.4	5	0.0538	8.5	8.3%
Cocos	19.5	233.8	0.9911	4.9	3.4	64	0.0531	59.9	$<1\times10^{-16}$
Capricorn	21.6	33.6	0.5801	9.5	5.4	121	0.0435	56.0	$<1\times10^{-16}$
Eurasia	−71.2	304.1	0.0472	63.8	51.4	167	0.0418	3.2	72.0%
India	26.7	15.2	0.4598	11.6	6.9	113	0.0458	44.0	$<1\times10^{-16}$
Juan de Fuca	−42.3	61.4	1.1925	3.7	3.0	91	0.0571	17.7	$<1\times10^{-16}$
Lwandle	6.0	341.6	0.1185	35.5	26.9	116	0.0518	11.9	7.7%
Macquarie	38.2	19.1	1.0560	5.1	2.9	112	0.0468	66.8	$<1\times10^{-16}$
North America	−63.6	317.4	0.2568	20.6	13.2	156	0.0403	22.8	$<1\times10^{-16}$
Nubia	1.5	335.8	0.1343	31.7	24.5	122	0.0527	9.4	**3.3**%
Nazca	39.9	263.0	0.4522	8.1	7.8	84	0.0639	43.1	$<1\times10^{-16}$
Pacific	−63.4	100.3	0.8890	4.7	3.8	4	0.0602	88.9	$<1\times10^{-16}$
Philippine Sea	−54.3	341.2	1.0676	5.2	3.3	136	0.0389	79.7	$<1\times10^{-16}$
Rivera	18.2	252.9	4.3365	1.0	0.7	58	0.0608	18.9	$<1\times10^{-16}$
South America	−81.8	72.5	0.2569	18.6	13.0	37	0.0511	26.2	$<1\times10^{-16}$
Scotia	−85.4	350.8	0.1568	30.1	20.6	119	0.0472	8.7	**0.4**%
Somalia	22.5	308.4	0.1237	27.4	24.8	70	0.0663	13.1	27.8%
Sur	−80.1	68.4	0.2740	17.7	12.2	42	0.0514	17.4	$<1\times10^{-16}$
Sundaland	26.3	289.6	0.1037	31.1	27.5	45	0.0683	6.2	51.2%
Sandwich	−37.8	329.7	1.4560	3.7	2.4	145	0.0411	55.8	$<1\times10^{-16}$
Yangtze	77.3	202.6	0.0870	45.8	34.7	88	0.0475	8.6	24.6%
NNR-MORVEL	−57.1	68.6	0.2529	16.7	13.8	58	0.0573		**7.3**$\times$**10**$^{-6}$
Microplates									
Aegean Sea	−37.1	93.4	0.2839	12.4	11.7	136	0.0664	31.3	**1.4**$\times$**10**$^{-4}$
Altiplano	−36.0	285.9	0.4559	11.3	7.2	7	0.0479	16.9	$<1\times10^{-16}$
Anatolia	28.8	31.8	1.1776	4.7	2.7	120	0.0440	22.6	$<1\times10^{-16}$
Balmoral Reef	−66.2	114.8	0.7123	6.1	4.6	164	0.0595	71.6	$<1\times10^{-16}$
Banda Sea	−6.2	119.2	2.5744	1.5	1.3	168	0.0646	39.6	$<1\times10^{-16}$
Birds Head	−44.7	94.8	1.0311	3.5	3.3	170	0.0654	93.3	$<1\times10^{-16}$
Burma	−12.1	284.0	2.1502	2.1	1.5	16	0.0588	46.1	$<1\times10^{-16}$
Caroline	−68.2	70.6	0.8528	5.4	4.1	45	0.0551	94.4	$<1\times10^{-16}$
Conway Reef	−23.4	168.4	3.9784	1.2	0.8	76	0.0535	57.1	$<1\times10^{-16}$
Easter	23.7	67.5	11.3716	0.5	0.3	139	0.0490	48.2	$<1\times10^{-16}$
Futuna	−18.8	176.5	5.1223	1.0	0.6	71	0.0495	65.6	$<1\times10^{-16}$
Galapagos	0.3	80.9	5.6158	0.8	0.6	139	0.0596	36.6	$<1\times10^{-16}$
Juan Fernandez	33.6	70.7	22.3628	0.2	0.1	143	0.0468	77.8	$<1\times10^{-16}$
Kermadec	34.8	10.2	2.2728	2.3	1.4	108	0.0484	42.9	$<1\times10^{-16}$
Manus	−3.9	150.1	51.6031	0.1	0.1	59	0.0556	72.5	$<1\times10^{-16}$
Maoke	−1.4	89.0	0.8780	4.8	3.5	143	0.0620	73.8	$<1\times10^{-16}$
Mariana	1.6	132.3	1.3376	3.1	2.7	31	0.0595	53.2	$<1\times10^{-16}$
Molucca Sea	−1.3	305.8	3.4873	1.2	1.0	165	0.0611	29.5	$<1\times10^{-16}$
New Hebrides	−4.3	356.4	2.5143	2.1	1.4	120	0.0435	109.8	$<1\times10^{-16}$
Niuafo'ou	−7.1	183.4	3.2726	1.6	1.0	64	0.0445	61.9	$<1\times10^{-16}$
North Andes	−78.5	105.4	0.1808	24.8	17.9	0	0.0538	19.1	**0.2**%
North Bismarck	−50.0	117.7	1.0677	3.6	3.0	146	0.0651	96.4	$<1\times10^{-16}$

Table 4. (continued)

Plate	Angular Velocity			Standard Error Ellipse			σ_ω°/Ma^{-1}	v_{RMS} mm a^{-1}	$p(\chi^2)_0$
	°N	°E	°/Ma^{-1}	σ_{max}	σ_{min}	ζ_{max}			
Okhotsk	−50.0	301.3	0.1267	37.0	25.1	171	0.0420	4.7	**2.1%**
Okinawa	31.4	124.4	2.4647	2.1	1.4	22	0.0463	37.0	**<1×10^{-16}**
Panama	19.4	243.6	0.1419	32.8	20.9	45	0.0492	11.1	**2.6%**
Shetland	−3.3	162.6	0.0903	43.6	33.8	62	0.0506	9.6	24.6%
Solomon Sea	−9.5	126.7	1.7943	2.0	2.0	24	0.0643	86.5	**<1×10^{-16}**
South Bismarck	5.4	329.1	8.0643	0.6	0.4	120	0.0565	38.2	**<1×10^{-16}**
Timor	−10.3	110.7	1.9903	1.9	1.6	150	0.0663	58.6	**<1×10^{-16}**
Tonga	24.5	5.4	8.9070	0.6	0.4	110	0.0479	98.6	**<1×10^{-16}**
Woodlark	−6.6	124.8	1.8293	2.0	1.9	7	0.0639	77.7	**<1×10^{-16}**

[a]SKS-MORVEL is identical to SKS-GV-MORVEL. NNR-MORVEL is a set of angular velocities, constrained by the MORVEL relative angular velocities, of the 25 MORVEL plates in a reference frame in which there is no net rotation of the lithosphere [*Argus et al.*, 2011]. Probabilities less than 5% are printed in bold, which indicate that the differences are statistically significant. ζ_{max} is the azimuth of the major axis of the error ellipse. $p(\chi^2)_0$ is the probability of obtaining data as different or more different as those used in SKS-MORVEL if the angular velocity of the plate is zero. The covariance matrix of SKS-MORVEL in Cartesian coordinates is

$$\begin{bmatrix} \sigma_{xx}^2 & \sigma_{yx}^2 & \sigma_{zx}^2 \\ \sigma_{xy}^2 & \sigma_{yy}^2 & \sigma_{zy}^2 \\ \sigma_{xz}^2 & \sigma_{yz}^2 & \sigma_{zz}^2 \end{bmatrix} = \begin{bmatrix} 5806 & -2012 & 1912 \\ -2012 & 11630 & -3290 \\ 1912 & -3290 & 7183 \end{bmatrix} \times 10^{-10} \ rad^2 \ Ma^{-2}$$

4.2. Plate Velocities

The MORVEL angular velocities describe the relative motions of 25 major plates and can be compactly summarized by 24 angular velocities while one plate is arbitrarily held fixed, which *DeMets et al.* [2010] choose to be the Pacific plate. Thus, MORVEL contains no information about how the 25 major plates move relative to the deep mantle, which requires one additional angular velocity to describe. In SKS-MORVEL, that one additional angular velocity is specified entirely by the two-tier least squares fit to the orientations of seismic anisotropy inferred from shear wave splitting.

In SKS-MORVEL, the angular velocities of eight of 25 major plates (i.e., those included by *DeMets et al.* [2010]) differ insignificantly from zero: the Amur ($p = 51.8\%$), Antarctica ($p = 88.4\%$), Caribbean ($p = 8.3\%$), Eurasia ($p = 72.0\%$), Lwandle ($p = 7.7\%$), Somalia ($p = 27.8\%$), Sundaland ($p = 51.2\%$), and Yangtze ($p = 24.6\%$) plates (Table 4 and Figures 9 and 10). (Here p is the probability of obtaining data as different or more different from those used in SKS-MORVEL if the angular velocity of that plate is zero.) v_{RMS} for these eight plates range from 2 to 13 mm a^{-1} (Table 4). In every case the relative angular velocity between each plate pair differs significantly from zero, so not more than one of these plates can be truly motionless. Within the uncertainties of specifying a frame of reference for absolute plate velocities, however, the angular velocities of these eight plates cannot be resolved from zero.

Among the 25 major plates, the fastest-moving plates are the Pacific, Philippine Sea, Australia, Macquarie, Cocos, Capricorn, and Sandwich plates, with v_{RMS} ranging from 89 to 56 mm a^{-1} (Table 4 and Figures 8–10). As has been observed for prior realizations of absolute plate velocities, plates with large continental area tend to move slower than oceanic plates [*Minster et al.*, 1974]. Among the 31 additional plates incorporated by *Argus et al.* [2011] from *Bird* [2003], v_{RMS} ranges from a low of 5 mm a^{-1} for the Okhotsk plate to a high of 110 mm a^{-1} for the New Hebrides plate, making it the fastest-moving plate on the planet (Table 4). The values of v_{RMS} that we find are generally lower than those found by *Cuffaro and Jurdy* [2006], who estimated velocities of microplates relative to the hot spots by combining the relative plate motions of *Bird* [2003] with the absolute motion of the Pacific plate from *Gripp and Gordon* [2002]; their estimates of v_{RMS} range from 14 mm a^{-1} for the Galapagos plate to 132 mm a^{-1} for the New Hebrides plate.

The sizes of the uncertainties of the angular velocities for different plates are similar to one another (Table 4). Thus, the ratio between the size of the uncertainty to the size of the rotation rate for a slow-moving plate is much larger than the ratio for a fast-moving plate. The uncertainty of the plate motion direction for the slow-moving
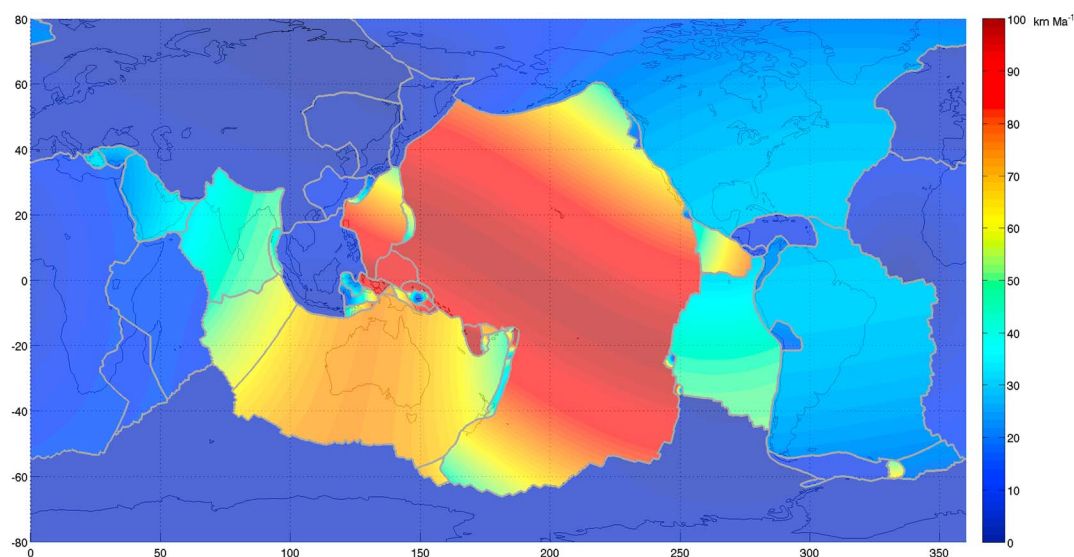
Figure 8. Plate speed relative to the subasthenospheric mantle in SKS-MORVEL SKS-MORVEL (equivalent to SKS-GV-MORVEL; all plates, v_{RMS} weighted). The motion of eight major plates (Amur, Antarctica, Caribbean, Eurasia, Lwandle, Somalia, Sundaland, and Yangtze plates) differs insignificantly from zero. Miller cylindrical projection.

plates is therefore also larger than that for the fast-moving plates. For the slow-moving plates, such as the Antarctica plate, the direction of absolute plate motion in most places cannot be resolved at the 95% confidence level (Figures 9 and 10).

4.3. Comparison With Prior Results

There are two key differences between the present analysis and that of *Kreemer* [2009]. First, the absolute angular velocities of *Kreemer* [2009] were constrained to consistency with geodetically constrained plate motions, while ours are constrained to consistency with MORVEL, which causes some small differences in results. Second, and more importantly, the confidence limits that we find here are roughly 2 orders of magnitude larger than found by *Kreemer* [2009]. Within these larger uncertainties, the two sets of angular velocities are mutually consistent except for the Nazca plate for which the relative angular velocities are very different (Figures 6 and 10).

The angular velocities relative to the hot spots estimated by *Morgan and Phipps Morgan* [2007] also lie within the 95% confidence regions of SKS-MORVEL (Figures 6 and 10). In contrast, the angular velocities that we estimate here, except for SKS-CV-MORVEL, are generally inconsistent with the HS3-NUVEL1A angular velocities [*Gripp and Gordon*, 2002], which indicate a higher rate of rotation of the Pacific plate (Figure 6). Thus, our results are consistent with the hypothesis of *Morgan and Phipps Morgan* [2007] that biases in volcanic propagation rate data used by *Gripp and Gordon* [2002] may induce a small bias in HS3-NUVEL1A that results in a velocity of the Pacific plate that is too high.

4.4. Net Rotation of the Lithosphere

To estimate the net rotation of the lithosphere, we compare SKS-MORVEL with NNR-MORVEL56, which is a set of 56 plate angular velocities, constrained to consistency with the MORVEL relative plate angular velocities, in a reference frame in which there is no net rotation of the lithosphere [*Argus et al.*, 2011]. The comparison indicates a significant right-handed net rotation of the entire lithosphere of $0.25° \pm 0.11°$ Ma^{-1} about a pole at 57.1°S, 68.6°E (Figure 7).

Gripp and Gordon [2002] estimated a higher net rotation of $0.44 \pm 0.11°$ Ma^{-1} relative to the hot spots. The 95% confidence limits of these net rotations overlap but differ significantly (Figure 7). Plate driving force models predict the net rotation of the entire lithosphere relative to the subasthenosphere mantle. *Cocksworth and Harper* [1996] estimated the net rotation of the lithosphere from their plate driving force model, and *Gripp and Gordon* [2002] revised the result to be consistent with NUVEL-1A. This revised plate driving force model indicates a net rotation of $0.25°$ Ma^{-1} right handed about a pole of (59°S, 48°E), which is contained in the 95% uncertainty limits of SKS-MORVEL (Figure 7).
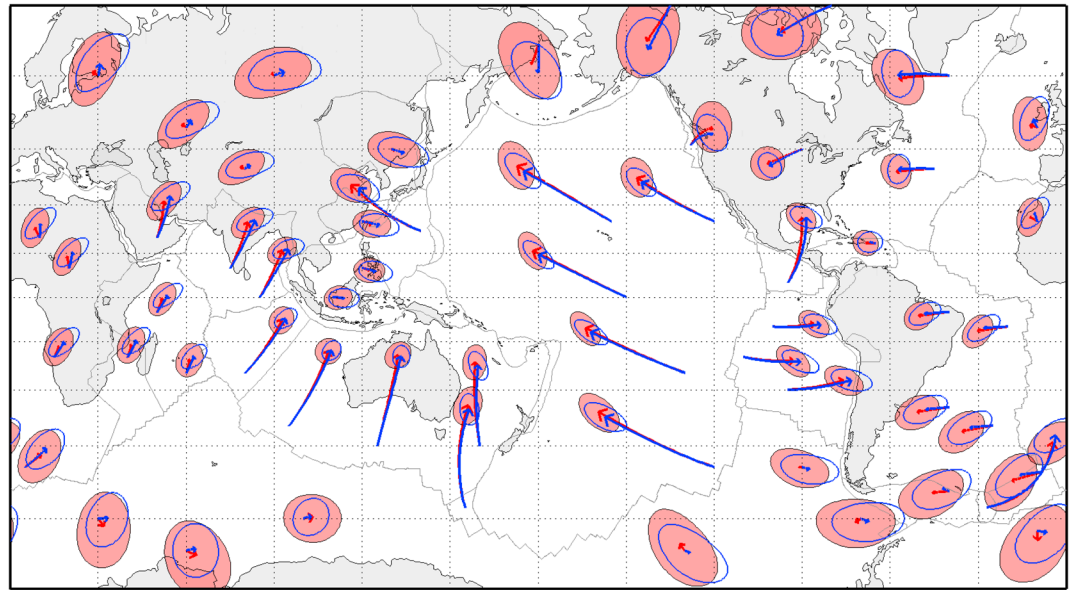
Figure 9. Absolute plate motions from SKS-MORVEL (red, equivalent to SKS-GV-MORVEL; all plates, v_{RMS} weighted) and SKS-OV-MORVEL (blue, oceanic plates, v_{RMS} weighted). Each arrow shows the displacement path of a point on a plate if the plate were to maintain its current angular velocity for 40 Ma. Ellipses show the 2-D 95% confidence ellipse of velocity multiplied by 40 Ma. Mercator's projection.

Given the consistency between our estimated plate angular velocities and those of *Morgan and Phipps Morgan* [2007] from the trends of hot spot tracks, we believe that SKS-MORVEL is a reliable estimate of the motion of the plates relative to the subasthenospheric mantle. While the no net rotation frame of reference is convenient and is used by many geoscientists, we—along with many others—believe that it does not indicate the motion of the plates relative to the subasthenospheric mantle.
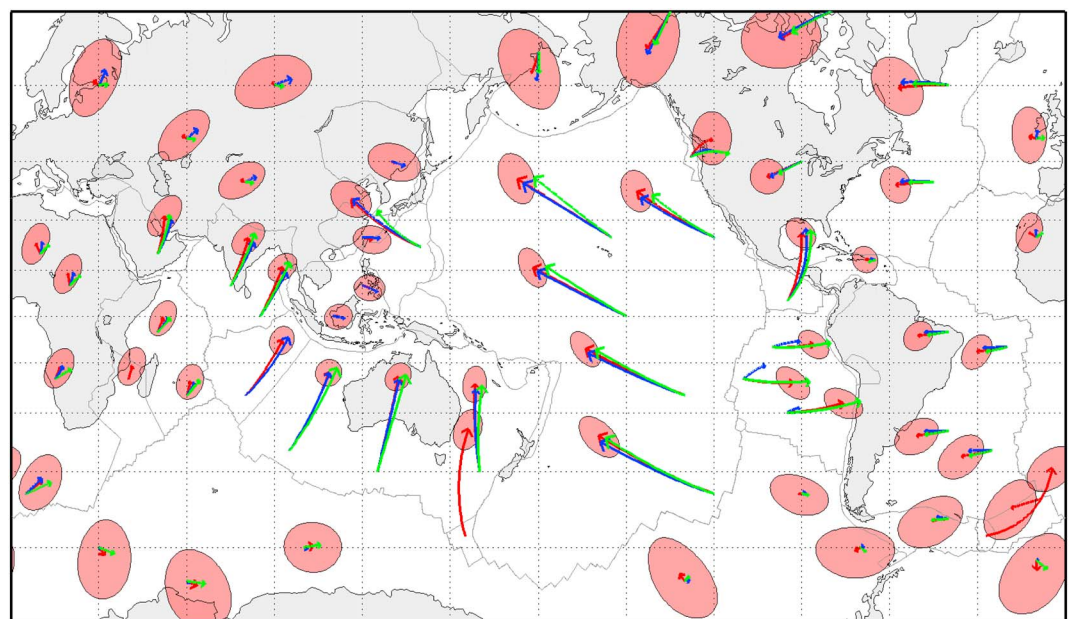

Figure 10. Absolute plate motions from SKS-MORVEL (red, equivalent to SKS-GV-MORVEL; all plates, v_{RMS} weighted), from *Kreemer* [2009] (blue), and from *Morgan and Phipps Morgan* [2007] (green). Each arrow shows the displacement path of a point on a plate if the plate were to maintain its current angular velocity for 40 Ma. Ellipses show the 2-D 95% confidence ellipse of velocity multiplied by 40 Ma. Mercator's projection.
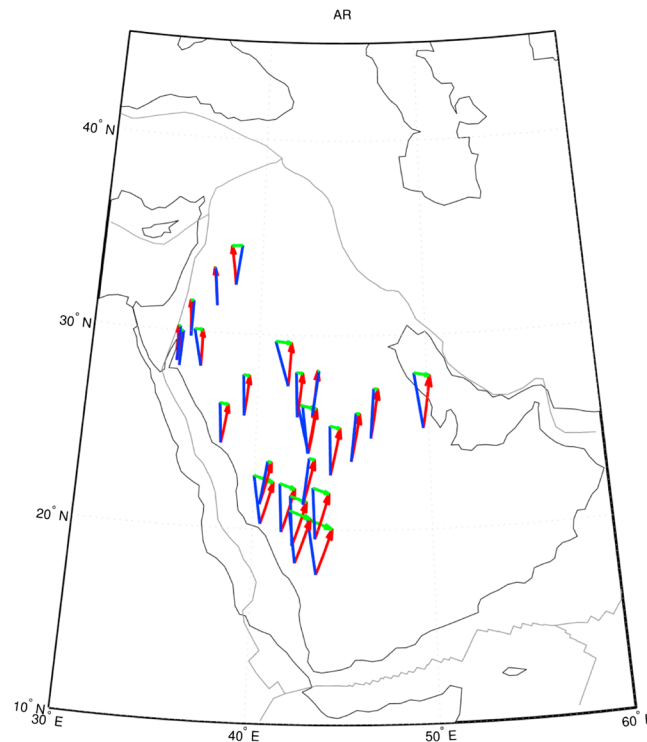
Figure 11. Observed (blue) orientations or shear wave splitting compared with the direction of plate motion (red arrows, which show 10 Ma of displacement from SKS-MORVEL) for the Arabia plate. The green arrows show the discrepancy projected onto the direction perpendicular to the plate motion. In 19 out of 25 cases the red arrows are clockwise of the observed orientations, possibly indicating a component of asthenospheric flow toward the E-SE, with a mean velocity of 6 mm a^{-1}. Equidistant conic projection.

4.5. Flow in the Asthenosphere

The strong correlations in azimuth residuals identified in this paper may be influenced by flow in the asthenosphere. If so, the sense of misfit provides constraints on the direction and rate of flow in the asthenosphere. For example, the direction of motion of the Arabia plate indicated in SKS-MORVEL is in 19 out of 25 cases clockwise of the observed azimuths (Figure 11). This general trend implies that a component of the superposed mantle flow beneath the Arabia plate is toward the east-southeast, with the mean velocity being 6 mm a^{-1}. Alternatively, the systematic difference might be caused by anisotropy in the mantle lithosphere.

5. Conclusions

1. Errors in azimuths inferred from shear wave splitting are correlated within any one plate. The neglect of this correlation resulted in unrealistically small confidence limits in prior estimates of absolute plate velocities. For example, we estimate that the 95% confidence limits on Pacific plate absolute motion from seismic anisotropy are $\approx \pm 0.15°$ Ma^{-1}, more than 2 orders of magnitude larger than found before.

2. The within-plate dispersion for oceanic lithosphere, $\sigma = 19.2°$, differs insignificantly from that for continental lithosphere, $\sigma = 21.6°$.

3. The between-plate angular standard deviation for continental lithosphere, $\sigma = 14.7°$, is significantly greater than the between-plate angular standard deviation for oceanic lithosphere, $\sigma = 7.4°$. Consequently, the confidence limits of the angular velocities constrained by oceanic data are always more compact than those constrained by continental data.

4. The angular velocities estimated from equal weighting and from v_{RMS} weighting differ insignificantly when using the same data set. The angular velocities constrained by oceanic data are less sensitive to the choice of weighting scheme than are the continental data.

5. SKS-MORVEL (equivalent to SKS-GV-MORVEL), our preferred set of angular velocities, indicates a net rotation of the entire lithosphere of $0.25° \pm 0.11°$ Ma^{-1} about a pole of 57.1°S, 68.6°E. This net rotation is consistent with that indicated by plate driving force models.

6. In SKS-MORVEL, the motion relative to the subasthenospheric mantle of the Amur, Antarctica, Caribbean, Eurasia, Lwandle, Somalia, Sundaland, and Yangtze plates differs insignificantly from zero.

7. Two of the slowest plates, Antarctica ($v_{RMS} = 4$ mm a^{-1}, $\sigma = 29°$) and Eurasia ($v_{RMS} = 3$ mm a^{-1}, $\sigma = 33°$), have two of the largest within-plate dispersions, which may indicate that a plate must move faster than ~ 5 mm a^{-1} for millions of years to result in seismic anisotropy useful for estimating plate motion. The anisotropy observed beneath plates moving as slowly as 9 mm a^{-1} (v_{RMS}) may be useful for estimating the direction of plate motion relative to the subasthenospheric mantle.

References

Adam, J. M. C., and S. Lebedev (2012), Azimuthal anisotropy beneath southern Africa from very broad-band surface-wave dispersion measurements, *Geophys. J. Int.*, *191*, 155–174, doi:10.1111/j.1365-246X.2012.05583.x.

Argus, D. F., R. G. Gordon, and C. DeMets (2011), Geologically current motion of 56 plates relative to the no-net-rotation reference frame, *Geochem. Geophys. Geosyst.*, *12*, Q11001, doi:10.1029/2011GC003751.

Barklage, M., D. A. Wiens, A. Nyblade, and S. Anandakrishnan (2009), Upper mantle seismic anisotropy of South Victoria Land and the Ross Sea coast, Antarctica from SKS and SKKS splitting analysis, *Geophys. J. Int.*, *178*, 729–741, doi:10.1111/j.1365-246X.2009.04158.x.

Becker, T. W. (2008), Azimuthal seismic anisotropy constrains net rotation of the lithosphere, *Geophys. Res. Lett.*, *35*, L05303, doi:10.1029/2007GL032928.

Behn, M. D., C. P. Conrad, and P. G. Silver (2004), Detection of upper mantle flow associated with the African Superplume, *Earth Planet. Sci. Lett.*, *224*, 259–274, doi:10.1016/j.epsl.2004.05.026.

Bird, P. (2003), An updated digital model of plate boundaries, *Geochem. Geophys. Geosyst.*, *4*(3, 1027), doi:10.1029/2001GC000252.

Chase, C. G. (1972), The n-plate problem of plate tectonics, *Geophys. J. R. Astron. Soc.*, *29*, 117–122, doi:10.1111/j.1365-246X.1972.tb02202.x.

Chase, C. G. (1979), Asthenospheric counterflow: A kinematic model, *Geophys. J. R. Astron. Soc.*, *56*, 1–18, doi:10.1111/j.1365-246X.1979.tb04764.x.

Cocksworth, G. R., and J. F. Harper (1996), Plate driving forces, *Research Report*, vol. 96–196, pp. 18, Mathematics Dept., Victoria Univ. of Wellington, Wellington, New Zealand.

Conrad, C. P., and M. D. Behn (2010), Constraints on lithosphere net rotation and asthenospheric viscosity from global mantle flow models and seismic anisotropy, *Geochem. Geophys. Geosyst.*, *11*, Q05W05, doi:10.1029/2009GC002970.

Conrad, C. P., M. D. Behn, and P. G. Silver (2007), Global mantle flow and the development of seismic anisotropy: Differences between the oceanic and continental upper mantle, *J. Geophys. Res.*, *112*, B07317, doi:10.1029/2006JB004608.

Cuffaro, M., and D. M. Jurdy (2006), Microplate motions in the hotspot reference frame, *Terra Nova*, *18*, 276–281, doi:10.1111/j.1365-3121.2006.00690.x.

Debayle, E., and Y. Ricard (2013), Seismic observations of large-scale deformation at the bottom of fast-moving plates, *Earth Planet. Sci. Lett.*, *376*(0), 165–177, doi:10.1016/j.epsl.2013.06.025.

Debayle, E., B. Kennett, and K. Priestley (2005), Global azimuthal seismic anisotropy and the unique plate-motion deformation of Australia, *Nature*, *433*(7025), 509–512.

DeMets, C., R. G. Gordon, D. F. Argus, and S. Stein (1990), Current plate motions, *Geophys. J. Int.*, *101*, 425–478, doi:10.1111/j.1365-246X.1990.tb06579.x.

DeMets, C., R. G. Gordon, and D. F. Argus (2010), Geologically current plate motions, *Geophys. J. Int.*, *181*, 1–80, doi:10.1111/j.1365-246X.2009.04491.x.

Fouch, M. J., and S. Rondenay (2006), Seismic anisotropy beneath stable continental interiors, *Phys. Earth Planet. Inter.*, *158*, 292–320, doi:10.1016/j.pepi.2006.03.024.

Gordon, R. G., and A. Cox (1980), Calculating paleomagnetic poles for oceanic plates, *Geophys. J. Int.*, *63*, 617–640, doi:10.1111/j.1365-246X.1980.tb02642.x.

Gripp, A. E., and R. G. Gordon (1990), Current plate velocities relative to the hotspots incorporating the NUVEL-1 global plate motion model, *Geophys. Res. Lett.*, *17*, 1109–1112, doi:10.1029/GL017i008p01109.

Gripp, A. E., and R. G. Gordon (2002), Young tracks of hotspots and current plate velocities, *Geophys. J. Int.*, *150*, 321–361, doi:10.1046/j.1365-246X.2002.01627.x.

Irving, E. (1964), *Paleomagnetism and its Application to Geological and Geophysical Problems*, pp. 399, John Wiley, New York.

Jupp, P. E. (2001), Modifications of the Rayleigh and Bingham tests for uniformity of directions, *J. Multivar. Anal.*, *77*, 1–20, doi:10.1006/jmva.2000.1922.

Kreemer, C. (2009), Absolute plate motions constrained by shear-wave-splitting orientations with implications for hot spot motions and mantle flow, *J. Geophys. Res.*, *114*, B10405, doi:10.1029/2009JB006416.

Kreemer, C., D. A. Lavallée, G. Blewitt, and W. E. Holt (2006), On the stability of a geodetic no-net-rotation frame and its implication for the International Terrestrial Reference Frame, *Geophys. Res. Lett.*, *33*, L17306, doi:10.1029/2006GL027058.

Long, M. D., and T. W. Becker (2010), Mantle dynamics and seismic anisotropy, *Earth Planet. Sci. Lett.*, *297*, 341–354, doi:10.1016/j.epsi.2010.06.036.

Mardia, K. V., and P. E. Jupp (1999), *Directional Statistics*, Wiley, New York.

Marone, F., and B. Romanowicz (2007), The depth distribution of azimuthal anisotropy in the continental upper mantle, *Nature*, *447*(7141), 198–201.

Minster, J. B., T. H. Jordan, P. Molnar, and E. Haines (1974), Numerical modeling of instantaneous plate tectonics, *Geophys. J. R. Astron. Soc.*, *36*, 541–576, doi:10.1111/j.1365-246X.1974.tb00613.x.

Morgan, W. J. (1972), Plate motions and deep mantle convection, *Mem. Geol. Soc. Am.*, *132*, 7–22.

Morgan, W. J., and J. Phipps Morgan (2007), Plate velocities in the hotspot reference frame, in *Plates, Plumes, and Planetary Processes*, vol. 430, edited by G. R. Foulger and D. M. Jurdy, pp. 65–78, Geol. Soc. of Am., Boulder, Colo., doi:10.1130/2007.2430(04).

Savage, M. K. (1999), Seismic anisotropy and mantle deformation: What have we learned from shear-wave-splitting?, *Rev. Geophys.*, *37*, 65–106, doi:10.1029/98RG02075.

Silver, P. G. (1996), Seismic anisotropy beneath the continents: Probing the depths of geology, *Annu. Rev. Earth Planet. Sci.*, *24*, 385–432, doi:10.1146/annurev.earth.24.1.385.

Silver, P. G., S. S. Gao, K. H. Liu, and the Kaapval Seismic Group (2001), Mantle deformation beneath southern Africa, *Geophys. Res. Lett.*, *28*, 2493–2496, doi:10.1029/2000GL012696.

Silver, P. G., M. J. Fouch, S. S. Gao, and M. Schmitz (2004), Seismic anisotropy, mantle fabric, and the magmatic evolution of Precambrian southern Africa, *S. Afr. J. Geol.*, *107*, 45–58, doi:10.2113/107.1-2.45.

Silver, P. G., M. Behn, K. Kelley, M. Schmitz, and B. Savage (2006), Understanding cratonic flood basalts, *Earth Planet. Sci. Lett.*, *245*, 190–201, doi:10.1016/j.epsl.2006.01.050.

Tommasi, A., B. Tikoff, and A. Vauchez (1999), Upper mantle tectonics: Three-dimensional deformation, olivine crystallographic fabrics and seismic properties, *Earth Planet. Sci. Lett.*, *168*, 173–186, doi:10.1016/S0012-821X(99)00046-1.

Wadsworth, G. P. (1960), *Introduction to Probability and Random Variables*, vol. 52, McGraw-Hill, New York.

Yuan, H., and B. Romanowicz (2010), Lithospheric layering in the North American craton, *Nature*, *466*(7310), 1063–1068, doi:10.1038/nature09332.

Zhang, S., and S. Karato (1995), Lattice preferred orientation of olivine aggregates deformed in simple shear, *Nature*, *375*, 774–777, doi:10.1038/375774a0.